Chapter 7
Multislice Applications and Examples

Abstract The multislice method of calculating electron microscope images of thicker specimen is applied to several different specimen. First, some simple examples are worked through to help understand how to use the method and then some more complicated specimens are investigated to illustrate the method.

The multislice method simulates electron transmission in a thick specimen including dynamical scattering. Chapter 6 presented the theory of the multislice method and discussed how to use it in general terms. This chapter will gives some specific examples of performing a multislice simulation. The examples serve to illustrate some typical multislice results and also provide a more detailed description of using the multislice method.

A prerequisite for image simulation is a detailed description of the coordinates of the atoms in the specimen. The two volume set of Wyckoff [385] is a good starting point for many common materials with a crystalline structure. The books by Megaw [241] and Vainshtein et al. [350,351] give a thorough discussion of crystal structure. There are also numerous journal articles (see for example the journal Acta Cryst.) with crystal structure information.

7.1 Gallium Arsenide

Gallium Arsenide (GaAs) is a relatively simple structure similar to that of silicon (the diamond structure) except that adjacent atoms alternate between gallium and arsenic in the zinc sulfide (or zincblende) structure. The cubic lattice constant is slightly bigger (5.65Å) than that of silicon (5.43Å) so that it may be slightly easier to image in the electron microscope. However, the atoms in GaAs are significantly heavier (atomic number $Z = 31$ and 33 for Ga and As, respectively) and scatter

E.J. Kirkland, *Advanced Computing in Electron Microscopy*,
DOI 10.1007/978-1-4419-6533-2_7,

more strongly than silicon (Z = 14). GaAs may be expected to have more dynamical scattering than silicon, so a simple phase grating calculation (as in Chap. 5) may not be sufficient. This is a good place to start testing the multislice method because this specimen may produce significant dynamical scattering but is relatively simple to describe.

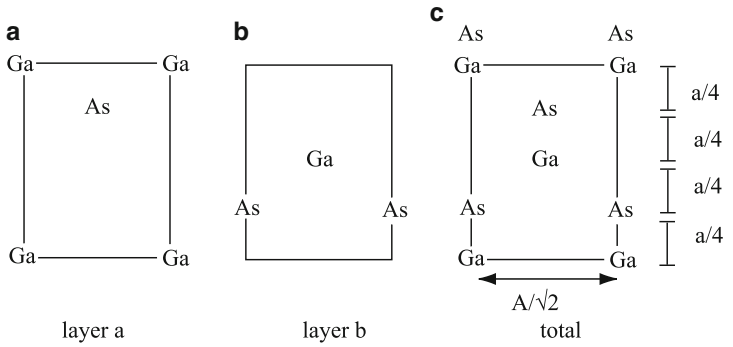

Fig. 7.1 The structure of gallium arsenide (GaAs) projected along the 110 direction. GaAs has a zincblende structure with a cubic lattice constant of $a_{GA} = 5.65$Å. (a) and (b) are two different atomic layers suitable for use in a multislice calculation and (c) is the projection of whole specimen. The layers are stacked in the sequence *ababa*.... Each layer is 1.998Å thick (along z or the optic axis) and 3.995 × 5.65Å in x and y (in the plane of the paper)

In the 110 projection GaAs has a projected structure as shown in Fig. 7.1. The main difference between silicon (Fig. 5.15) and GaAs is that there are two different types of atoms (Ga and As). In the 110 projection, GaAs naturally divides into two different layers as (labeled a and b in Fig. 7.1). The layers are stacked in the sequence *ababa*... with a spacing along the z axis (optic axis) of $\sqrt{2}a_{GA}/4 = 1.9976$Å. Silicon can be divided in the same manner if the Ga and As atoms are replaced with Si and the lattice constant is changed. It is best to use these two layers as the slices in the multislice method. The thickness is small enough to get an accurate answer (which is usually the case for the natural layers in a small unit cell crystal) and using the natural layers of the specimen will ensure that the multislice simulation correctly reproduces the HOLZ (or upper layer lines) portion of the diffraction patterns. Although the HOLZ lines may not contribute directly to a BF CTEM phase image of a thin specimen, getting the HOLZ lines correct is frequently required for an accurate simulation of thick specimens in BF (to get the phase of the low order reflections correct) and is usually required for ADF-STEM images because the ADF detector collects large scattering angles (where the HOLZ lines are). The actual atomic coordinates for each layer are shown in Table 7.1.

Table 7.1 The normalized coordinates for two layers in one projected unit cell of the (110) projection of GaAs

Atom	Layer	x/a_0	y/b_0
Ga	a	0	0
As	a	0.5	0.75
As	b	0	0.25
Ga	b	0.5	0.5

The two dimensional unit cell dimensions are $a_0 \times b_0$ where $a_0 = a_{GA}/\sqrt{2} = 3.995$Å and $b_0 = a_{GA} = 5.65$Å. a_{GA} is the cubic lattice constant of GaAs

7.1.1 BF-CTEM Simulation

Once the structure of the specimen has been determined and a convenient way of layering or slicing the specimen has been identified, the next step is to find the correct sampling for the simulation. The general guidelines for simulating thin specimens (Table 5.4) are a good starting point. Dynamical scattering in a thick specimen will also introduce further constraints on the sampling. The easiest way to discover these sampling requirements is to simply try a range of super cell sizes with different numbers of pixels. A sequence of trial multislice runs (using an incident plane wave) is shown in Table 7.2 for two different thickness of 110 GaAs. The super cell sizes were chosen to yield a reciprocal space sampling size of about one mrad. at 200 keV to get adequate sampling inside the objective aperture. The columns labeled "Intensity" refer to the total integrated intensity in the final electron wave function at the exit surface of the specimen. As discussed in Sect. 6.10.2 the integrated intensity should remain constant at unity if there is adequate sampling. Typically this value will decrease with thickness but should not go below about 0.90 for a reasonable simulation, and a value of 0.95 or higher is typical for a good simulation. Table 7.2 shows that this simulation probably needs about 512×512 pixels (or more) to simulate a thickness of 200 Å.

The magnitude $|\psi(x,y)|$ of the electron wave function $\psi(x,y)$ after passing through a thickness of 10(ab) and 50(ab) layers (40 and 200 Å) is shown in Fig. 7.2. An ideal perfect microscope with amplitude contrast would produce an image similar to that in Fig. 7.2. A phase grating calculation (as in Chap. 5) would yield identically $|\psi(x,y)| = 1$ across the whole area because it approximates the transmission process as a pure phase shift. Figure 7.2 illustrates that the specimen is not a pure phase object. The electron intensity accumulates near the atom sites (a white spot in Fig. 7.2). The imaging electrons see a large positive charge at the atom nucleus that is screened by the bound electrons of the atom. Far away from the atom the imaging electrons (at 200 keV in this example) do not see any net charge (for neutral atoms the positive charge on the nucleus equals the number of negatively charged bound electrons), but near the nucleus the imaging electrons see the large positive charge on the nucleus and are attracted to the center of the atoms in the specimen. The

Table 7.2 The effects of sampling on a multislice calculation of 110 GaAs

Unit cells	Size (in Å)	Number of pixels	Max angle (mrad)	Intensity at 10(ab)	Intensity at 50(ab)
$5a_0 \times 3b_0$	19.98×16.95	128×128	53.6	0.969	0.821
”	”	256×256	107.1	0.987	0.906
”	”	512×512	214.3	0.997	0.978
$6a_0 \times 4b_0$	23.97×22.2	128×128	44.6	0.964	0.802
”	”	256×256	89.3	0.980	0.871
”	”	512×512	178.6	0.995	0.967
$7a_0 \times 5b_0$	27.97×28.25	128×128	37.9	0.967	0.812
”	”	256×256	75.8	0.975	0.849
”	”	512×512	151.5	0.993	0.951
$8a_0 \times 6b_0$	31.96×33.9	128×128	31.6	0.969	0.807
”	”	256×256	63.1	0.972	0.834
”	”	512×512	126.3	0.991	0.938
”	”	1024×1024	252.5	0.998	0.982

The two-dimensional unit cell dimensions are $a_0 = a_{GA}/\sqrt{2} = 3.995$Å and $b_0 = a_{GA} = 5.65$Å. a_{GA} is the cubic lattice constant for GaAs. 10(ab) means that there are 10 repeats of both the a and b layers (about 40Å thick). 50(ab) results in a thickness of about 200Å

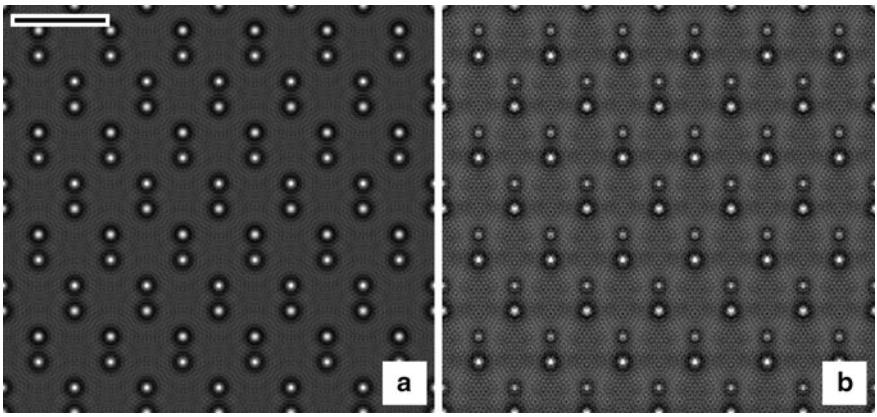

Fig. 7.2 The magnitude of the electron wave function $|\psi(x,y)|$ (in real space) after passing through (a) 40Å and (b) 200Å of 110 GaAs at an electron energy of 200 keV. The super cell size is $6a_0 \times 4b_0$ with 512×512 pixels. The scale bar in (a) is 5 Å. The numerical range of each image is (a) 0.18–3.70 and (b) 0.01–3.30 (*white is a larger positive number*)

imaging electrons effectively get channeled into the atomic columns in the specimen. The black ring surrounding each atom site is a depletion of electron intensity.

Channeling is not a static process either. As the imaging electrons progress further through the specimen they may be scattered out of the atomic column as well. Figure 7.2b shows this effect. The As atoms have a slightly larger positive charge on the nucleus. The white spot at the As sites is less bright than the white spot at the Ga sites indicating that the imaging electrons are diminishing in intensity at the As

sites. This is a dynamical scattering effect. The relative intensities of the channeling peaks on the Ga and As sites will likely oscillate with thickness. There is a faint structure in the magnitude of the electron wave function that looks like standing waves between the atom sites. This occurs when the HOLZ lines appear and it is not always clear whether this is the real space manifestation of the HOLZ lines or simply a sampling error.

Figure 7.3 show the intensity and phase of the $k_x = k_y = 0$ Fourier coefficient (or zero order beam) of the wave function of the electron as it is passing through the specimen. Both the intensity and the phase oscillate with depth, clearly indicating the dynamical nature of the scattering process. All of the nonzero Fourier coefficients or beams will oscillate with depth, although with a different period. The period of oscillation is referred to as the extinction depth for the particular beam (or Fourier coefficient). The dynamical nature of the scattering process is completely lacking in a phase grating calculation (as in Chap. 5) and the multislice calculation (or equivalently a Bloch wave calculation) is required to correctly simulate strongly scattering specimen (more than about 10–20 Angstroms in the case of 110 GaAs).

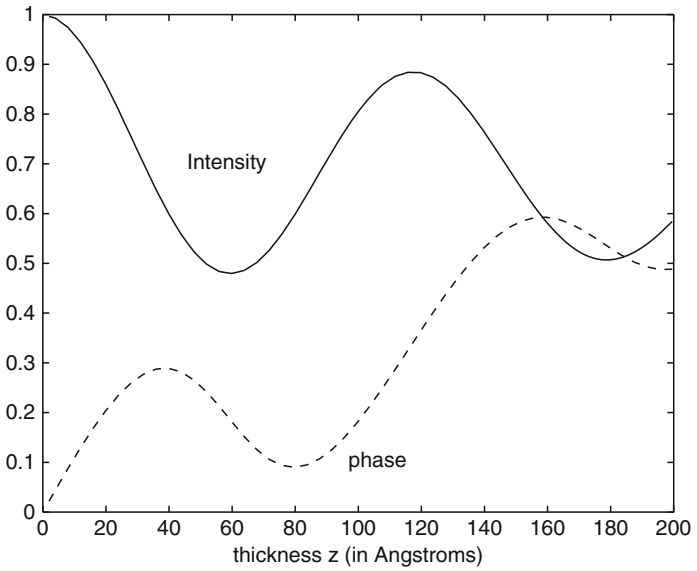

Fig. 7.3 The intensity and phase of the $k_x = k_y = 0$ Fourier coefficient of the 200 keV electron wave function as it passes through the 110 projection of GaAs. The super cell size is $6a_0 \times 4b_0$ with 512×512 pixels

The simulated bright field (BF) phase contrast image is shown in Fig. 7.4 for various thickness of the specimen. Scherzer conditions were used for the defocus and partial coherence was approximately included using the transmission cross

coefficient (Sect. 5.4.3). Figure 7.4a is for two layers of the specimen and is approximately the same as a phase grating calculation. Each pair of atoms (Ga and As) in the dumbbell appears a a black ellipse. Figure 7.4b is for a slightly thicker crystal. The relative phases of the Fourier coefficients have already changed significantly. Some features that should be white are black and vice versa. The image has a lot of artifacts and the overall periodicity is double of what it should be. These artifacts can vary dramatically with small changes in defocus and the size of the objective aperture. Figure 7.4c is a thick crystal. Although the overall periodicity is again correct there has been a contrast reversal. This illustrates why image simulation is necessary to interpret a high-resolution phase contrast image.

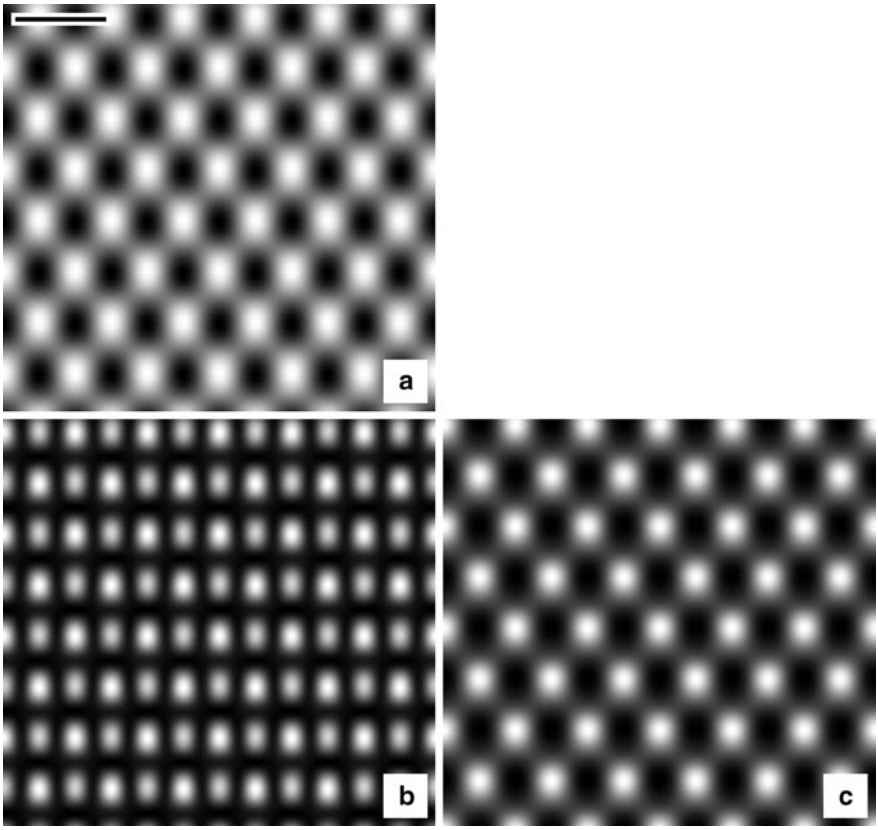

Fig. 7.4 Simulated bright field phase contrast images for different thickness of 110 GaAs at 200 keV. $C_s = 1.3$ mm, $\Delta f = 700$Å, obj. apert. 12 mrad, with partial coherence (1 mrad spread in illumination and 100 Å defocus spread). (a) 4 Å (2 layers), (b) 40 Å (20 layers), and (c) 200 Å (100 layers). The super cell size is $6a_0 \times 4b_0$ with 512×512 pixels. The range of each image is (a) 0.91–1.09, (b) 0.57–1.07, (c) 0.247–1.48 (*white is a larger positive number*)

7.1.2 ADF-STEM Simulation

The annular dark field (ADF) STEM image is a small signal (compared to phase contrast BF) and directly involves high angle scattering. Both of these effects are more difficult to calculate and an ADF-STEM image simulation requires more attention to the accuracy and tolerance of the calculation (i.e., sampling requirements). Finding the super cell size and number of pixels to achieve a total integrated intensity of nearly unity (as in Table 7.2) is the first requirement. It is also a good idea to test the accuracy more directly. This is conveniently done by comparing two different simulations with slightly different sampling. If the sampling is adequate then there should be no difference between using $N_x \times N_y$ pixels and $2N_x \times 2N_y$ pixels with a similar real space super cell size. There are two different sampling requirements that should be tested. The pixel size (and number of pixels) in both real space and reciprocal space is important. The number of pixels is restricted to powers of two (for the FFT) so the two simulations must differ by a factor of two in the number of pixels. If the real space super cell size were left the same then the sampling in real space (Δx and Δy) would double however the pixel size in Fourier or reciprocal space ($\Delta k_x = 1/a$ and $\Delta k_y = 1/b$) would remain the same. To vary both at the same time the super cell size should be increased by about a factor of $\sqrt{2}$ (within the constraints of the specimen periodicity) to get approximately the same reduction in the pixel size in both real space and reciprocal space.

Figure 7.5 shows a comparison between two different simulations with different sampling sizes on the 110 projection of GaAs. This is only a test of the sampling, so a full image simulation is not necessary. An ADF-STEM multislice simulation requires a full multislice calculation for each position of the scanned probe which can require a lot of computer time. A simple one dimensional line scan through an appropriate feature of the specimen is usually sufficient to test the sampling, but requires substantially less computer time. Figure 7.5 shows a scan through adjacent Ga and As atoms along the direction of there closest position (vertical in Fig. 7.1). The low resolution simulation had a super cell size of $6a_0 \times 4b_0$ with 512×512 pixels and the high-resolution simulation had a super cell size of $8a_0 \times 6b_0$ with 1024×1024 pixels. There is a good agreement between the two curves so this sampling is probably adequate for performing the simulation. The difference between the two curves can also serve as an estimate of the sampling error in the simulation. The As atom is slightly heavier (Z = 33) than the Ga atom (Z = 31) so the peak on the As position is slightly higher (stronger scattering at the As position). Also, there is a slight peak in between the main dumbbells (at about y = 3.5Å in Fig. 7.5). This is caused by the tails of the probe (compare to Fig. 3.11).

Figure 7.6 shows the magnitude of the electron wave function $|\psi(x,y)|$ of the focused probe as it is passing through the specimen. The probe was positioned at an offset of (8Å,10Å) with (0,0) being in the lower left corner of the image. Although the initial probe is smooth and round the atomic columns of the specimen again attract the imaging electron which get channelled into the atomic columns. After a thickness of 200Å (Fig. 7.6b) the electron distribution in the probe can get fairly distorted by the specimen.

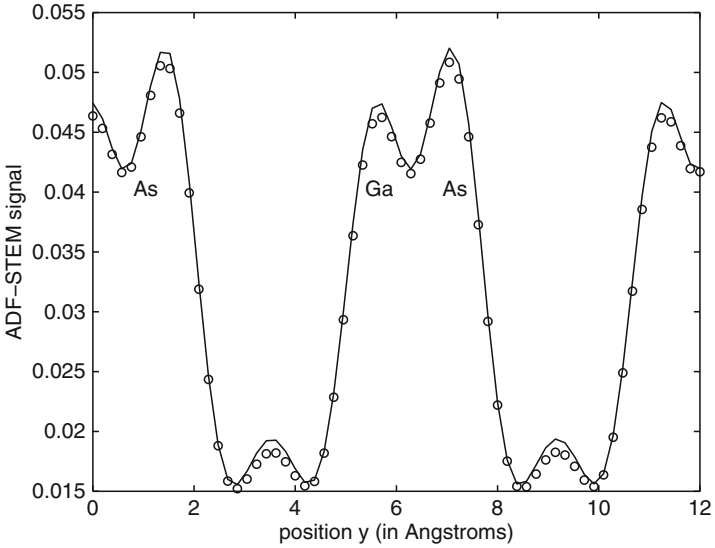

Fig. 7.5 Sampling test for ADF-STEM of 110 GaAs (40Å thick) at an electron energy of 200 keV. The curve shows the ADF signal in a *vertical line* through pairs of Ga and As atoms. The optical parameters were $C_s = 1.3$ mm, $\Delta f = 700$Å, with an objective aperture of 10.37 mrad. (Scherzer conditions). The ADF detector covered 40–175 mrad. The *solid curve* is for a super cell size of $8a_0 \times 6b_0$ with 1024×1024 pixels and the *circles* are for a super cell size of $6a_0 \times 4b_0$ with 512×512 pixels. The agreement between the two curves indicates that the sampling is sufficient

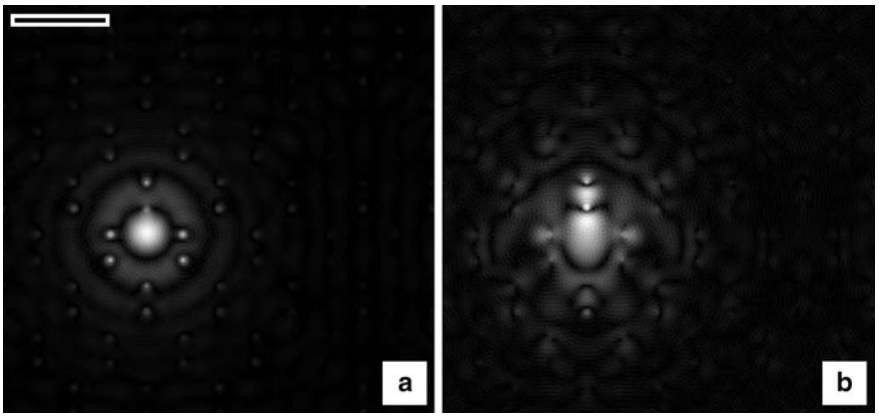

Fig. 7.6 The intensity distribution in the electron probe as it passes through 110 GaAs at an electron energy of 200 keV. (a) 40Å thick and (b) 200Å thick. The optical parameters were $C_s = 1.3$ mm, $\Delta f = 700$Å, with an objective aperture of 10.37 mrad. (Scherzer conditions). The super cell size had dimensions of $6a_0 \times 4b_0$ with 512×512 pixels. The range of each image is (a) 0.0–13.5, (b) 0.0–9.92 (*white is a larger positive number*). The scale bar in (a) is 5Å

The actual (simulated) ADF-STEM images calculated using the multislice method are shown in Fig. 7.7. These images require a multislice calculation for each point (or pixel) in the image. To save computer time only 32×32 pixels in one unit cell were calculated, and the unit cell was duplicated to fill the same area as the BF-CTEM simulation (Fig. 7.4). The specimen potential and electron wave function were each sampled with 512×512 pixels. The effective extinction distance for scattering to high angles (as on the ADF detector) is much larger than that for low angle scattering, which makes the ADF-STEM image much less sensitive to specimen thickness in the way that BF phase contrast is (compare to Fig. 7.4). The atomic columns are imaged as white in both the 40Å (Fig. 7.7a) and 200Å (Fig. 7.7b) images. The dumbbells are nearly resolved in these images. The magnitude of the ADF signal increases with thickness but there is not a contrast reversal as there was in BF phase contrast. The price paid for this improvement in image interpretation is a much smaller overall signal.

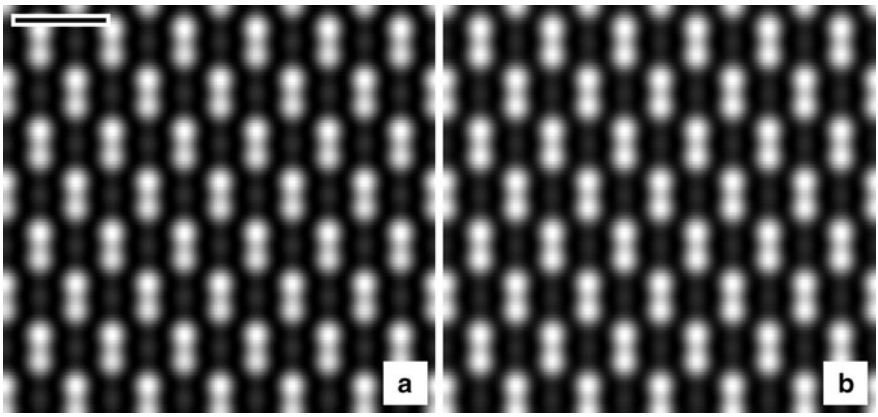

Fig. 7.7 Simulated ADF-STEM images of 110 GaAs at an electron energy of 200 keV for a thickness of (a) 40Å and (b) 200Å. The optical parameters were $C_s = 1.3$ mm, $\Delta f = 700$Å, with an objective aperture of 10.37 mrad. (Scherzer conditions). The specimen super cell size had dimensions of $6a_0 \times 4b_0$ with 512×512 pixels. The image was calculated as 32×32 pixels (in one unit cell) and periodically replicated to 96×64 pixels for display. *Black* is (a) 0.011, (b) 0.036 and *white* is (a) 0.051, (b) 0.144 where the total incident beam current is one. The scale bar in (a) is 5Å

7.1.3 Channeling

When the specimen is aligned along a major zone axis columns of atoms line up in a row along the optic axis. This is usually desirable because the atom columns may be imaged in their corresponding atomic location (in the 2D projection). As the electrons travel through the specimen they tend to channel along these atomic columns

in a process called channeling as is already evident in Figs. 7.2 and 7.6. This name can also apply to ion scattering in which the ions travel through the hollow space between atomic columns. Electrons are negatively charged and are attracted to the positive charge on the nucleus, so they tend to get pulled into the atomic columns and channel down a narrow channel that can be very small. The channeling width can be smaller than the outer electron shell in the atom and have a significant effect on low loss Electron Energy Loss Spectroscopy (EELS) signals (Kirkland [206]).

One advantage of a simulation is the ability to display signals that are not normally accessible in a real experiment. Figure 7.8a shows the electron intensity along a row of atom pairs in 110 GaAs vs. depth in the specimen (vertical direction) in an y,z plane (along a vertical line in Fig. 7.7) for an incident plane wave. An incident uniform plane wave is incident at the bottom of the image and exists the specimen at the top of the image (the electron wave is traveling up in this particular image). The channeling peak intensity increases significantly about half way through this specimen and then spreads out again as it travels further through the specimen. Channeling will oscillate with specimen thickness. The channeling peak will form (or oscillate) quicker with heavier atoms (and atom density along the beam) and lower electron energy. This particular example was chosen to reasonably fit on the page (low energy so it oscillates in a short distance). Channeling occurs in both fixed beam (CTEM) and scanned probe (STEM).

Figure 7.8b shows the channeling for an incident aberration correct probe placed in between atom pairs. The probe slowly gets pulled onto the atom cloumns as it passes through the specimen. Figure 7.8c is the same as (b) but with a saturated greyscale to bring out the low intensity portion of the image.

Channeling is sometimes an annoyance, but can be used to advantage. If the specimen (substrate) thickness is chosen so that the channeling peak is sharp and intense at the exist surface any atoms deposited on the exit surface will be strongly imaged only if they are on atomic columns but not in between, which may help distinguish where these atoms are.

In the Bloch wave picture, the electron eigenfunctions (or eigenvectors) have a high density near the atomic columns. In a two-dimensional plane perpendicular to the beam direction the electrons appear as states loosely bound to the atomic columns much like the lower energy atomic electrons are bound to the nucleus (but in this case the high energy beam electrons are bound to the screened nucleus). These states can be identified using atomic quantum numbers 1s, 1p, etc. (Kambe et al. [191] and Buxton et al. [44]) with similar symmetry. These eigenfunctions indicate a preference for propagation along the atomic columns (channeling). Pennycook and Jesson [283] were able to develop an intuitive understanding of ADF-STEM imaging based on the s-state eigenstates for well separated atomic columns. Anstits [14, 15] have shown that more states are needed for high resolution if the atomic columns are close. An atomic sized probe (with aberration corrector) placed on one atomic columns with another atomic column close by, may oscillate between columns as it propagated through the specimen.

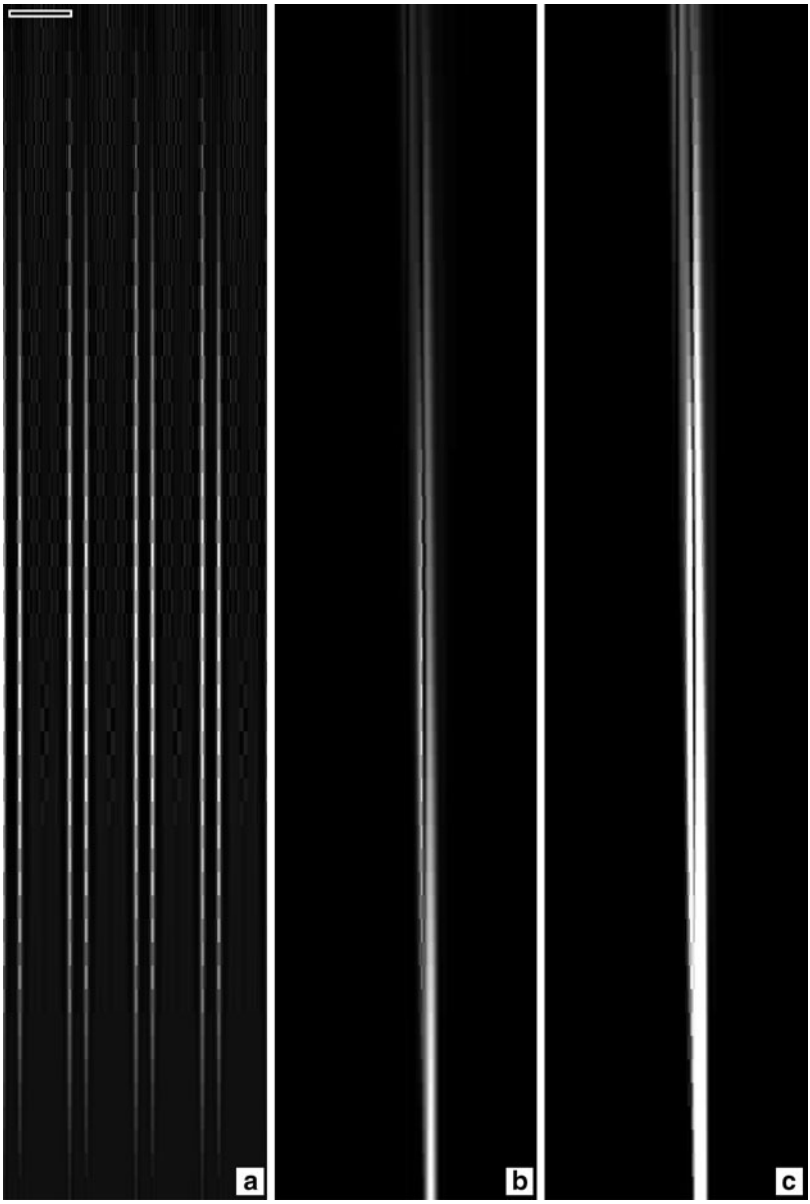

Fig. 7.8 Calculated electron intensity in 110 GaAs at an electron energy of 100 keV. (a) Plane wave incident. (b) Aberration corrected probe in between atom pairs ($C_{S3} = C_{S5} = \Delta f = 0$, objective aperture of 25 mrad). (c) same as (b) but with smaller *grey scale* range to bring out the low intensity portion of the image (*at top*). The specimen super cell size had dimensions of $6a_0 \times 4b_0$ with 512×512 pixels. The total thickness (*bottom to top*) was 100Å and the scale bar in (a) is 5Å

7.2 Silicon Nitride

Silicon nitride (specifically the β phase, β-Si_3N_4) has a hexagonal unit cell (Wyckoff [385]) as shown in Fig. 7.9. Each side of the unit cell is 7.606Å and there are two layer with a total repeat length of 2.909Å (perpendicular to the plane of the paper in Fig. 7.9). The hexagonal unit cell contains 14 atoms (6 silicon atoms and 8 nitrogen atoms).

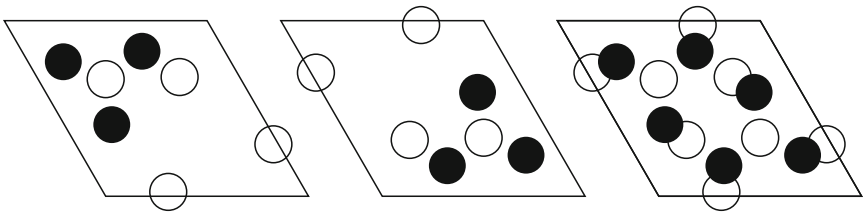

Fig. 7.9 The 001 projection of the hexagonal primitive unit cell of silicon nitride (β-Si_3N_4). The *open circles* are the positions of the nitrogen atoms and the *filled circles* are the positions of the silicon atoms. The a layer is on the *left*, the b layer is in the *middle* and the total projection is on the *right*. The *solid line* indicates the unit cell boundaries. The side of the unit cell is 7.606Å

Silicon nitride is an example of a more complicated unit cell that does not have rectangular symmetry. The multislice method of image simulation is most efficient when the FFT is used and the FFT is separable in x and y. This means that an FFT version of the multislice method works best with a rectangular unit cell. To simulate this specimen requires finding a larger unit cell with rectangular symmetry. One possible choice is shown in Fig. 7.10. The rectangular unit cell contains 28 atoms (12 silicon atoms and 16 nitrogen atoms). This particular specimen is easy to redefine a larger rectangular unit cell but an arbitrary specimen may be more difficult to describe this way. However, this step is required when using a multislice implementation using the FFT (required for an efficient calculation). Each specimen may require a different strategy to generate an equivalent rectangular unit cell.

Figure 7.11 shows the electron wave function after passing through about 50Å of the specimen. The magnitude in a) again shows that the electrons are attracted to the positively charged atomic nuclei and the specimen is not a pure phase object. The exit wave function, shown in b) and c) has both a strong real part and strong imaginary part. The complex transfer function of the objective lens can mix these two components in rather nonintuitive ways.

Figure 7.12 shows a simulated defocus series of silicon nitride with a thickness of 49.5Å (stacking sequence 17(ab)). The specimen was modeled as two layers with a stacking sequence of *ababa*.... The wave function and potentials were sampled with 256×256 pixels with a size of 38.03×39.52Å or $5a_0\times3b_0$ using the rectangular unit

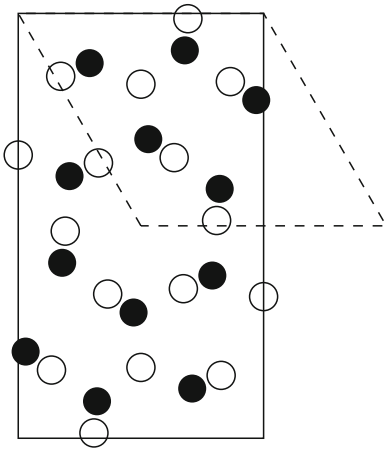

Fig. 7.10 The unit cell of silicon nitride (β-Si_3N_4) expanded to fill a rectangular area suitable for simulating using the multislice method with rectangular FFT's. The *open circles* are the positions of the nitrogen atoms and the *filled circles* are the positions of the silicon atoms. The position of the primitive hexagonal unit cell is shown as a *dashed line*. The unit cell has dimensions of $a_0 = 7.606$Å, and $b_0 = 13.174$Å, There are two layers each with a thickness of 1.4545Å

cell defined in Fig. 7.10 (maximum scattering angle of 54 mrad). Partial coherence was modeled using the transmission cross coefficient (see Sect. 5.4.3). The positions of the silicon atoms are initially black in Fig. 7.12a but reverse contrast as the defocus is changed, becoming white in Fig. 7.12b,c. Figure 7.13 shows the Scherzer focus image for two different thickness of the specimen. The apparent contrast of the silicon atom positions has reversed (black has become white). The sign of the contrast will changed periodically with defocus for a given thickness and also periodically with thickness for a given defocus, making image interpretation very difficult. Image simulation is one means of sorting out what is going on in the image.

An aberration corrected instrument will be corrected to some maximum angle or to some maximum order of aberration. The corrector will add a large negative C_{S3} to balance a large positive C_{S3} from the round objective lens. If the corrector is good to third order there will still be fifth order aberrations (C_{S50} plus all of the nonrotational aberrations), which may be minimized to some extent. Just as Scherzer used a lower order aberration (defocus) to partially compensate for the higher order C_{S3} aberration, the fifth order aberrations can be partially offset by the third order aberration. For simplicity ignore all of the rotational aberration like C_{32} etc. (which may be large and very important in practice). A third order corrector should be able to drive the total third order spherical aberration ($C_{S3} = C_{30}$) negative to partially offset the fifth order spherical aberration ($C_{S5} = C_{50}$). Similar pairs can be found in most of the rotational aberrations (left out from this discussion for simplicity). For example,

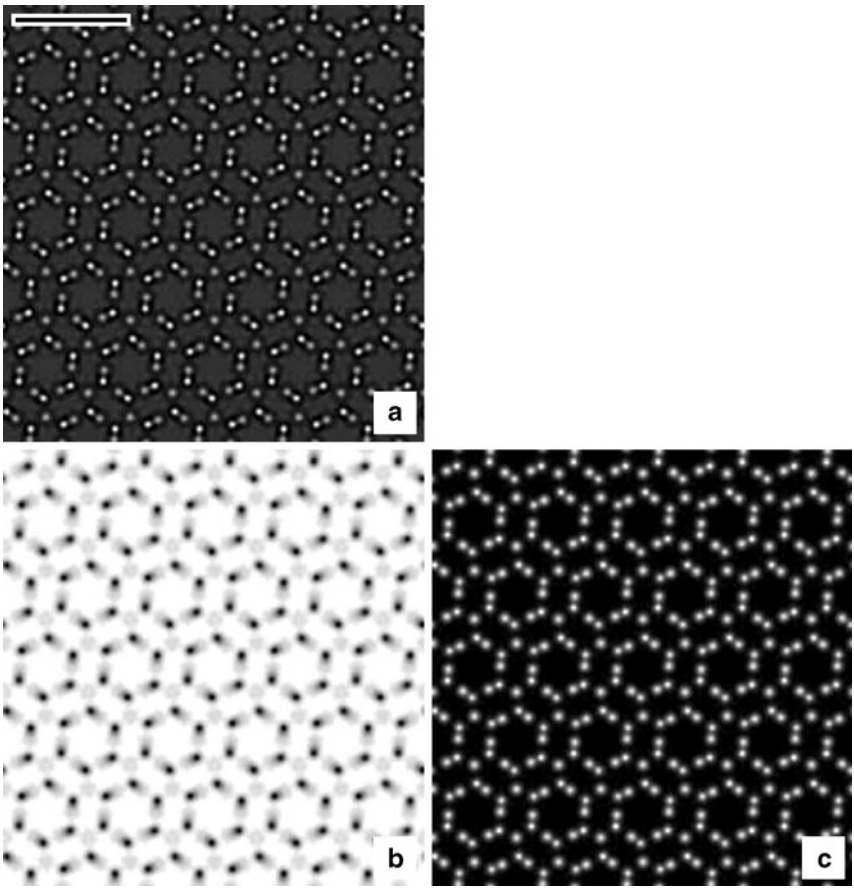

Fig. 7.11 The 200 keV electron wave function after passing through 49.5Å of 001 silicon nitride (β-Si_3N_4). (a) Magnitude $|\psi(x,y)|$ (b) Real part of $\psi(x,y)$ and (c) imaginary part of $\psi(x,y)$. The area of each image corresponds to 5×3 unit cells of the type shown in Fig. 7.10. The numerical range of each image is (a) 0.43–2.84, (b) −1.93–1.04 and (c) 0.01–2.27 (*white is a larger positive number*) The scale bar in (a) is 10Å

if $C_{S5} = 50$ mm is present at 200 kV then making a total $C_{S3} = -0.02$ mm allows the transfer function to go out to about 1Å (30 mrad) and look similar to that of Scherzer focus (Fig. 3.6).

Figure 7.14 shows Si_3N_4 calculated for an aberration corrected BF-CTEM with three different thickness using 512 by 512 pixels (maximum angle 108 mrad) and a slice thickness of 1.4545Å. The corrector is assumed to be good to third order out to an angle of 30 mrad. Figure 7.14a) is very thin (may not be possible in practice) and yields a good representation of the actual specimen structure. As the specimen gets thicker the atoms switch from black (expected) to white, which may be caused by an increase in the total phase as the electron wave passes through the specimen. At this high resolution the depth of focus is only about 30–40 Å (approximately

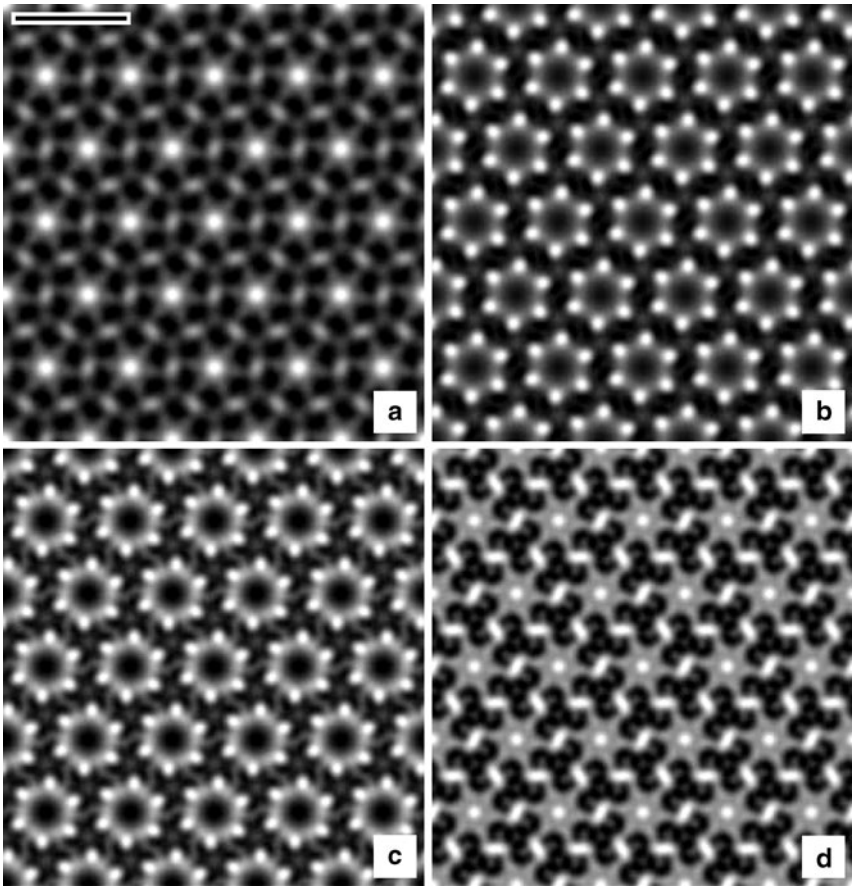

Fig. 7.12 Simulated CTEM defocus series of 001 silicon nitride (β-Si_3N_4), 49.5Å thick at a beam energy of 200 keV (C_s = 1.3 mm., obj. apert.=12 mrad, condenc. apert = 0.75 mrad, defocus spread = 100Å). The defocus values are (a) 700Å (Scherzer focus), (b) 900Å, (c) 1100Å and (d) 1300Å. The scale bar in (a) is 10Å . The area of each image corresponds to 5×3 unit cells of the type shown in Fig. 7.10. Silicon atom positions appear *black* in (a)

the resolution divided by the angle), which is less than the specimen thickness. In this calculation defocus is referred to the exit surface. Its not clear which plane is the optimum in this situation. Depth of focus becomes a significant problem as resolution increases. Jia et al. [188], Tillmann et al. [345] and Urban [348] have discussed other possible uses for negative C_{S3}.

Figure 7.15 shows a simulated ADF-STEM defocus series of silicon nitride under similar conditions to that in Fig. 7.12 except that the objective aperture was fixed at 10.37 mrad consistent with Scherzer conditions for a focused probe. The super cell size was $4a_0 \times 2b_0$ (or 30.4×26.3Å) with 512×512 pixels to allow a maximum scattering angle of 140 mrad (increased from the CTEM case in Fig. 7.12). The electron wave function was also sampled with 512×512 pixels. To save computer time

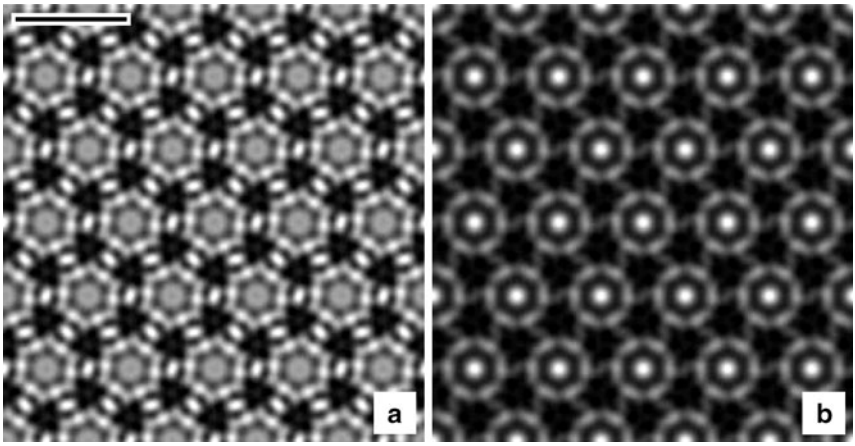

Fig. 7.13 Simulated CTEM images for two different thickness of 001 silicon nitride (β-Si_3N_4), at a beam energy of 200 keV (defocus of 700Å, C_s = 1.3 mm., obj. apert. = 12 mrad, condenc. apert = 0.75 mrad, defocus spread = 100Å). The specimen thickness was (a) 102Å (35(ab) layers), and (b) 151Å (52(ab) layers) The scale bar in (a) is 10Å . The area of each image corresponds to 5×3 unit cells of the type shown in Fig. 7.10

only the image in one rectangular unit cell was calculated with 32×64 pixels and replicated to fill the same area Fig. 7.12 for comparison. The silicon atom columns appear as white dots in Fig. 7.15a and do not reverse contrast unlike the BF phase contrast image, however there are still significant artifacts in the image that appear as the defocus is increased from Scherzer defocus ($\Delta f = 700$Å). The artifact are consistent with the tails of the probe. ADF-STEM is less sensitive to changes in defocus (than BF phase contrast) but there are still significant artifacts produced when defocus is changed. Figures 7.12 and 7.15 clearly indicate that the interpretation of a high-resolution image is not always straightforward in either BF-CTEM or ADF-STEM. Image simulation is one approach to verify that the image is interpreted correctly.

7.3 CBED Simulations

The CBED or Convergent Beam Electron Diffraction pattern is formed when a small focused probe is incident on the specimen. The diffraction pattern is from a microscopic area of the specimen and can also be referred to as the microdiffraction pattern. When the illuminating radiation is convergent (as required to focus on a small area of the specimen) then each diffraction spot is enlarged to the same size as the illumination cone and becomes a disk instead of a spot. The angular diameter of each disk is the same as the angular spread of the incident beam. In the case of the STEM each diffraction disk is the same size as the objective aperture.

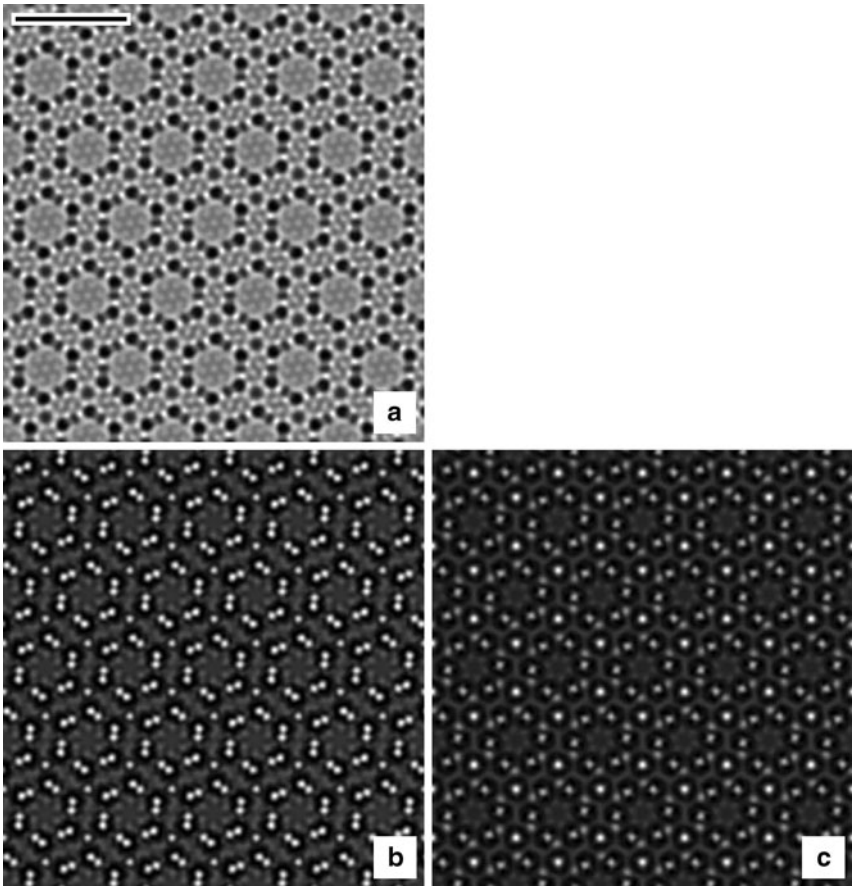

Fig. 7.14 Calculated aberration corrected BF-CTEM images for three different thickness of 001 silicon nitride (β-Si_3N_4), at a beam energy of 200 keV (defocus of 20Å, $C_{S5} = 50$ mm, $C_{S3} = -0.02$ mm, obj. apert. = 30 mrad, defocus spread = 10Å). The specimen thickness was (a) 22Å, (b) 100Å, and (c) 151Å. The scale bar in (a) is 10Å . The area of each image corresponds to 5×3 unit cells of the type shown in Fig. 7.10

The sampling error test (as in Table 7.2 and Fig. 7.5) are only an internal consistency test and do not test for systematic errors in the simulation theory or program implementation. The only real test of the simulation is a comparison to actual experimental data. Once the simulation software and theory have been verified by a detailed comparison to one or more experiments, then it can be used to predict other unknown situations.

Figure 7.16 shows experimentally recorded CBED patterns from 111 silicon at an electron energy of 100 keV (from Kirkland et al. [208]). In this case the probe (about 2.7Å diameter) is larger than the lattice spacing (1.92Å) so the CBED disks do not overlap and the lattice is not observable (Spence [332]). The outer

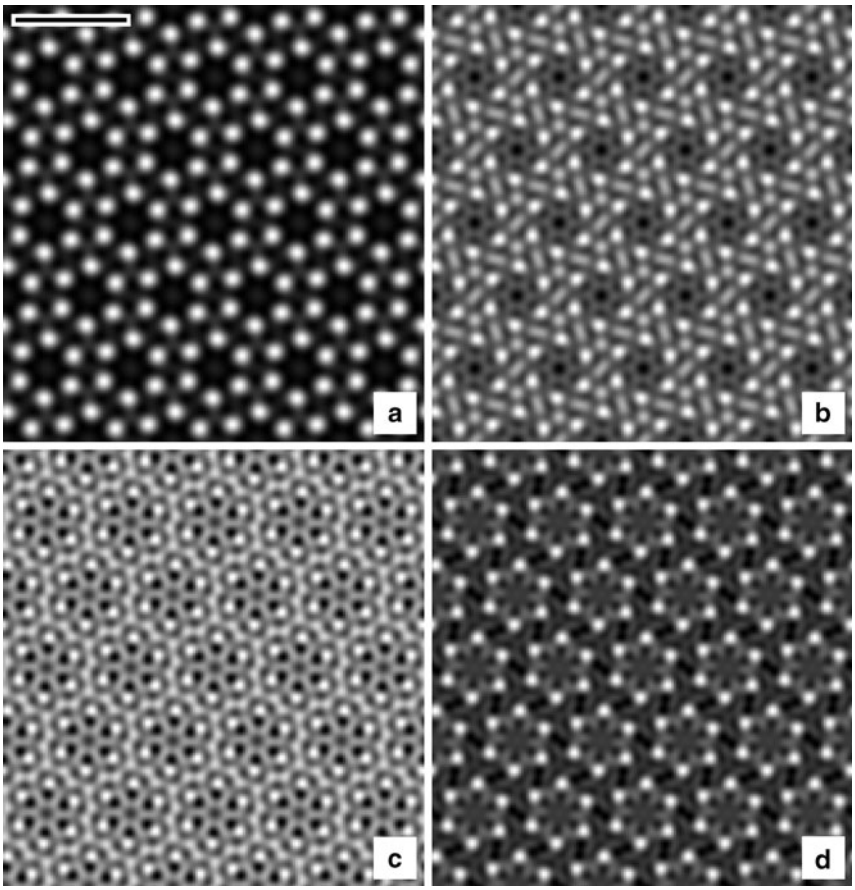

Fig. 7.15 Simulated ADF-STEM defocus series of 001 silicon nitride (β-Si_3N_4), 49.5Å thick at a beam energy of 200 keV (C_s = 1.3 mm, obj. apert. = 10.37 mrad). The defocus values are (a) 700Å (Scherzer focus), (b) 900Å, (c) 1100Å, and (d) 1300Å. The scale bar in (a) is 10Å . The area of each image corresponds to 5×3 unit cells of the type shown in Fig. 7.10. Silicon atom positions appear white in (a)

(white) ring is the HOLZ line. It is thin because the Ewald sphere intersects each diffraction disk at a steep angle. The patterns were recorded by photographing the diffraction screen (phosphor screen) with a 35 mm camera (using Kodak Plus-X film, chosen for its long linear region) with an exposure of 2 min. The dynamic range of the CBED pattern is too large to display easily so some old fashioned image processing was applied to the central seven disks (they were photographically *burned in* by a factor of six when the final prints were made in the dark room).

A CBED simulation requires only one multislice calculation like in a BF-CTEM calculation. The initial wave function is a focused probe (instead of a plane wave)

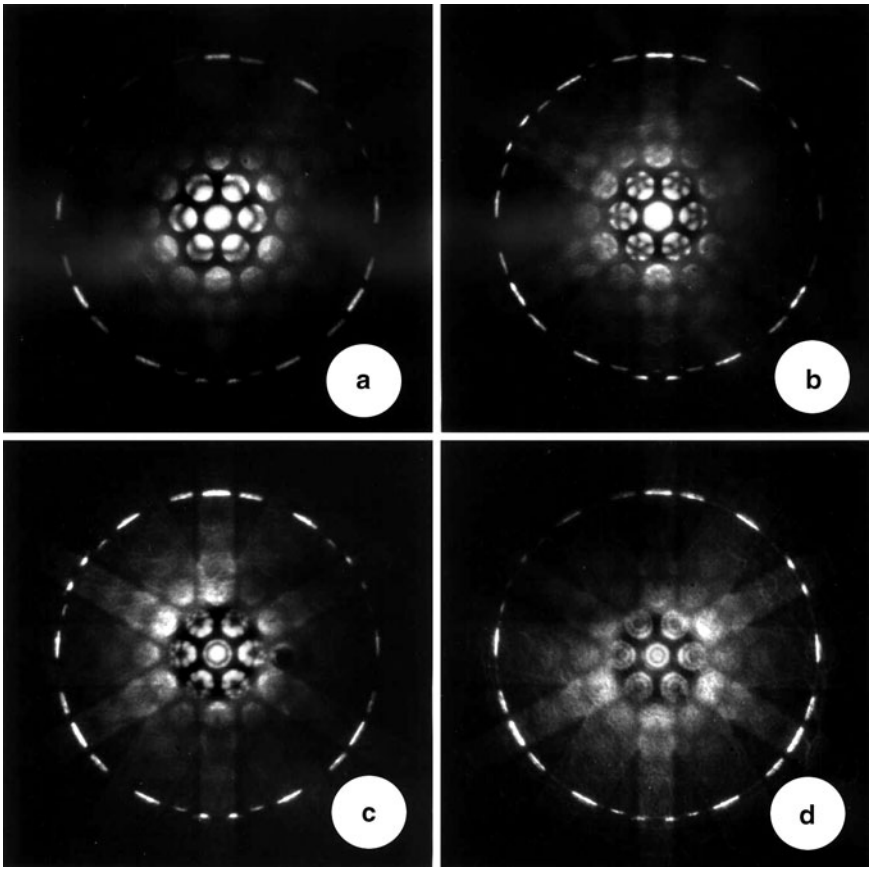

Fig. 7.16 Experimental CBED patterns of 111 silicon recorded in an HB501A STEM at 100 keV, $C_s = 3.3$ mm, with an objective aperture of 8 mrad. (Scherzer conditions). The specimen thickness was determined to be (a) 198 Å, (b) 273 Å, (c) 489 Å, (d) 1270 Å($\pm$30 Å). Reprinted from Kirkland et al. [208] with the permission of *The Minerals, Metals and Materials Society*

and the final image is Fourier transformed into the far field to get a diffraction pattern. Silicon 111 was modeled as a layered structure with a stacking sequence of *abcabca*.... The slice thickness (one layer per slice) is 3.135 Å, with a total repeat length of 9.405 Å. The wave function and specimen potential were sampled with 512×512 pixels and a super cell size of 53.5Å $\times$ 53.2Å. A library of CBED patterns was calculated for various thickness in the range 100–1500 Å at intervals of 10–50Å. Each experimental CBED pattern was visually matched to a simulated CBED pattern to determine the specimen thickness. It was possible to distinguish the thickness to an accuracy of about $\pm$30Å by observing the structure in the low order diffraction disks. The best match is shown in Fig. 7.17. Only the center two thirds of the diffraction pattern (342×342 pixels) is shown to avoid displaying the

portion that must be set to zero to eliminate aliasing. Note that the sampling in Fig. 7.17d) is not sufficient (the total integrated intensity dropped below 0.9) but it still reproduces the general features of the experiment.

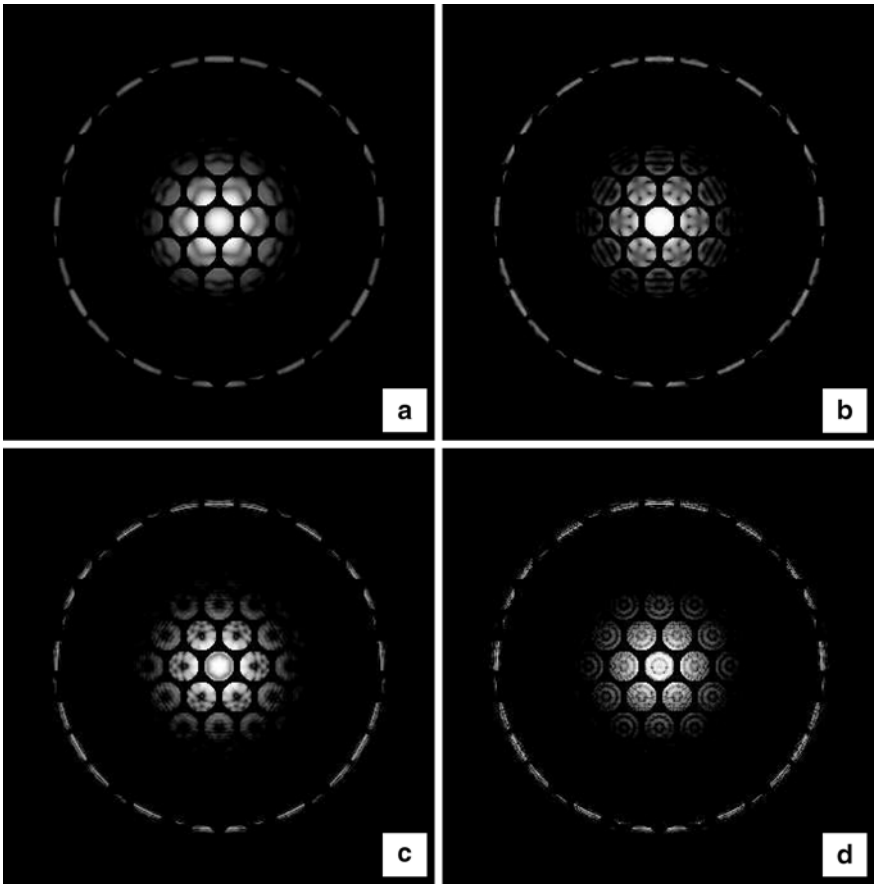

Fig. 7.17 Simulated CBED patterns of 111 silicon at 100 keV, $C_s = 3.3$ mm, with an objective aperture of 8 mrad. (Scherzer conditions). The specimen thickness was determined to be (a) 198 Å, (b) 273 Å, (c) 489 Å, (d) 1270 Å($\pm$30 Å). Each pattern is displayed on a logarithmic scale. The maximum scattering angle is 118 mrad. Reprinted from Kirkland et al. [208] with the permission of *The Minerals, Metals and Materials Society*

An EELS (Electron Energy Loss Spectroscopy) spectra was recorded for the same region that each CBED pattern was recorded. The ratio of the integrated signal in the first plasmon peak to the intensity in the zero loss peak is a good measure of the thickness of the specimen. Plotting the EELS ratio vs. the thickness determined by matching the CBED simulation yielded a straight line with a slope indicating

a plasmon mean free path of 1297 ± 25Å (with an EELS spectrometer collection angle of 8 mrad). The subjective agreement between Figs. 7.16 and 7.17 (overall features and the pattern of dark lines in the low order disks, taking into account the different intensity display scales used) and the measurement of the plasmon mean free path indicate a good agreement between the multislice simulation theory and an actual experiment. This particular experiment ignored the thermal motion of the atoms in the specimen. Later experiments by Loane et al. [228] yielded a plasmon mean free path of 1207Å including the effects of thermal atomic vibrations. The faint radial bands are called the Kikuchi bands and are also absent when thermal vibrations are ignored (as in Fig. 7.17).

7.4 Thermal Vibrations of the Atoms in the Specimen

All of the simulations considered so far have treated the atoms in the specimen as completely stationary. Most electron microscopy is done at room temperature of about 300°K (some microscopes can be equipped with heating and cooling stages). At room temperature the atoms in the specimen vibrate slightly. These atomic vibrations are quantized and the quantum unit of energy is called a phonon similar to the quantum unit of electromagnetic energy, the photon. Atomic vibrations are small compared to a typical interatomic distance so this effect is expected to be small but can lead to some interesting effects. In particular the thermal vibrations lead to a diffuse background intensity (in the diffraction pattern) in between the normal allowed diffraction positions. This type of scattering may be referred to as thermal diffuse scattering or simply TDS.

Typical optical phonons have a frequency no greater than about 10^{12} to 10^{13} Hz (Kittel [211]), and acoustic phonons are significantly lower frequencies. The imaging electrons in the microscope are traveling at about one half the speed of light (1.5×10^{10}cm/sec). At this speed it takes only about 0.7×10^{-16} s. to traverse the specimen which is much smaller than the period of oscillation of the atoms in the specimen. While the imaging electron is inside the specimen the atoms do not change their position significantly. The imaging electrons see the atoms as stationary but slightly offset from their normal lattice positions. The final image or diffraction pattern is made up of the average of many different imaging electrons. The typical current in the microscope is small enough that the time between two successive imaging electrons passing through the specimen is long compared to the period of oscillation of the thermal phonons in the specimen. Therefore, each successive imaging electron sees a slightly different configurations of atoms in the specimen. Each configuration of atoms is uncorrelated with all other configurations so the average over atomic configurations should be done incoherently.

The final image is the time average of many oscillations of the phonons in the specimen. However, only the imaging electron intensity and not the wave function can be averaged. This means that the time average must be performed in the image

plane (or diffraction plane if simulating a diffraction pattern) and not in the specimen plane. The detection process (film, CCD, etc.) converts the electron wave function into an intensity (square magnitude of the wave function). It is not appropriate to replace the atomic potential of the specimen by a time averaged potential (or equivalently apply a Debye-Waller factor to the atomic potential) because the phase of the imaging electron wave function must be carried through to the detector plane. It is only in the detector plane that the wave function can be converted to an intensity.

A general theory of imaging and diffraction in the presence of thermal vibrations can be rather involved (for example: Hall and Hirsch [142], Cowley and Pogany [65], Cowley and Murray [64], Rez et al. [301], Cowley [61], Allen and Rossouw [9], Wang and Cowley [369, 370], Wang [365–368], Dinges and Rose [79], Amali and Rez [12], Mitsuishi et al. [245], Dwyer and Etheridge [85], Croitoru et al. [70]). The theory of TDS scattering of X-rays has been thoroughly reviewed by Warren [371] and is very similar to TDS scattering of electrons. Although a theoretical analysis may be complicated there is however a simple if somewhat brute force approach to numerically simulate the effects of thermal vibrations in the specimen. Given a list of atomic coordinates in the specimen, offset the position of each atom by a small random amount and then perform a normal multislice simulation to get an image or diffraction pattern. Next repeat this process with a different random offset for each atomic coordinate (each random offset should start from the original unperturbed atom position, so the random offsets are not cumulative). The final image or diffraction pattern is the intensity averaged over several different configurations of atoms with different random offsets (average $|\psi|^2$ and not ψ). This approach is called the frozen phonon approximation (Loane et al. [227], Hillyard and Silcox [158]). The random offsets can be generated using a random number generator with a Gaussian distribution which is then equivalent to the Einstein model of the density of states for phonons (see for example Kittel [211]). This method can also be labeled a Monte-Carlo method because it uses a sequence of computer generated random numbers to perform a simulation. Fan [96], Dinges and Rose [79], and Amali and Rez [12] have proposed slightly different methods.

When all of the atoms in the specimen have a slightly different offset the specimen is no longer periodic in any direction. The specimen is technically amorphous although there is still an approximate periodicity. This simulation requires a different type of multislice simulation. Each slice of the specimen is different so there is no advantage to precalculating the slices, storing them and reusing the transmission function of each slice (they cannot be reused). This type of multislice simulation first reads in all of the coordinates (in practice the program reads in only the coordinates for one unit cell and then replicates them for many unit cells) and then adds a random offset for each coordinate. Then the atomic coordinates are sorted by depth and cut into thin slices. The transmission function for each successive slice is calculated (one at a time), applied to the transmitted wave function and then discarded because it cannot be used again.

7.4.1 Silicon 111 CBED with TDS

Thermal vibrations have the most visible effects on the diffraction pattern, generating a diffuse background intensity in between the normal diffraction spots. The steps in a frozen phonon calculation are shown in Fig. 7.18. Each atom was allowed to deviate from its normal lattice position with a Gaussian distribution and a standard deviation of 0.075Å in each of three directions, consistent with a measured Debye-Waller factor at room temperature (Sears and Selly [314]). This simulation models a CBED pattern ($|\Psi(k)|^2$) of the 111 projection of silicon. The wave function and potentials were sampled with 512×512 pixels in an area of 34.6×33.3Å (maximum scattering angle 183 mrad.). Figure 7.18a shows the CBED pattern without thermal displacements. Figure 7.18b has one particular set of random offsets. The number of different configurations in the average increases to 16 in figure 7.18d. Surprisingly, this is enough configurations to produce a smooth pattern. This calculation is completely elastic and there is no inelastic scattering.

This simulation in Fig. 7.18d should match the experimental CBED pattern in Fig. 7.16c. However, the scale was changed slightly to improve the sampling. The faint white bands that travel radially outward from the center of the CBED pattern are called the Kikuchi bands and are noticeably absent in the CBED simulation in Fig. 7.17 without thermal vibrations, but are reproduced appropriately in Fig. 7.18. Figure 7.19 shows the average intensity vs. scattering angle including thermal atomic vibrations. Notice that the intensity in between the diffraction peaks has become nonzero. The main effect of thermal vibrations is to reduce the intensity in the HOLZ lines and redistribute it more uniformly over the whole range of scattering angles. The ADF-STEM signal integrates over this whole region so there is only a small qualitative effect in the ADF-STEM image. The TDS should be included in ADF-STEM for a good quantitative calculation but usually does not have a qualitative effect on ADF-STEM image (Hillyard and Silcox [158]). Möbus et al. [249] have also added TDS to simulations of BF-CTEM images and conclude that there is no significant effect for thin specimen as are typically used. Recently, Muller et al. [257] have performed a more detailed simulation using a set of phonons accurately generated from the measured band structure of the crystal and found that there was no significant deviation from the simple Einstein model with a Gaussian distribution of atomic coordinate offsets. Debye-Waller factors for many different materials can be found in the literature (for example, Reid [293], Krishna and Sirdeshmukh [218] and Schowalter et al. [313])

7.4.2 Silicon 110 ADF-STEM with TDS

Generally speaking, the TDS scattering in crystalline specimens reduces the peak intensity in the Bragg peaks on the ADF detector. A significant portion reappears

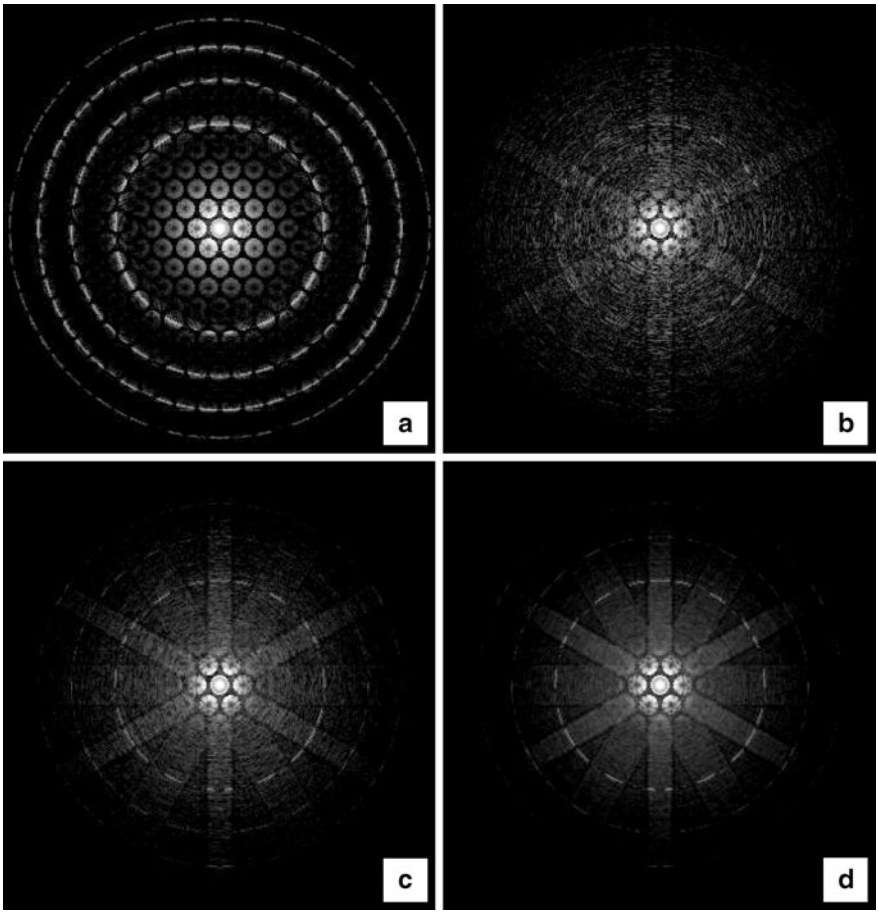

Fig. 7.18 Monte Carlo simulation of the CBED pattern of 111 silicon (489 Å thick) including thermal atomic vibrations (0.075Å in each direction) at 100 keV (C_s = 3.3 mm, obj. aperture 8 mrad. Scherzer conditions). (a) Has no thermal vibrations and the other images are the average of successively more sets of random displacements (b) one set, (c) four sets, and (d) 16 sets. Each pattern is displayed on a logarithmic scale. The maximum scattering angle is 183 mrad

as a diffuse background in between the Bragg peaks, which is still integrated by the ADF detector. Unless there are one or more strong Bragg peaks near the edge of the detector then TDS scattering should not have a large effect on the ADF-STEM image, although it should be included for a good quantitative comparison. Figure 7.20 shows a line scan through the so-called dumbbels (atom col. pair) in the 110 projection of Si (1.36 Å spacing) calculated with and without thermal vibrations (TDS scattering) for an aberration corrected 100 keV STEM. This calculation used 512 by 512 pixels with a super cell size of approximately 20 Å in each direction and a specimen thickness of about 100 Å. This super cell size includes scattering

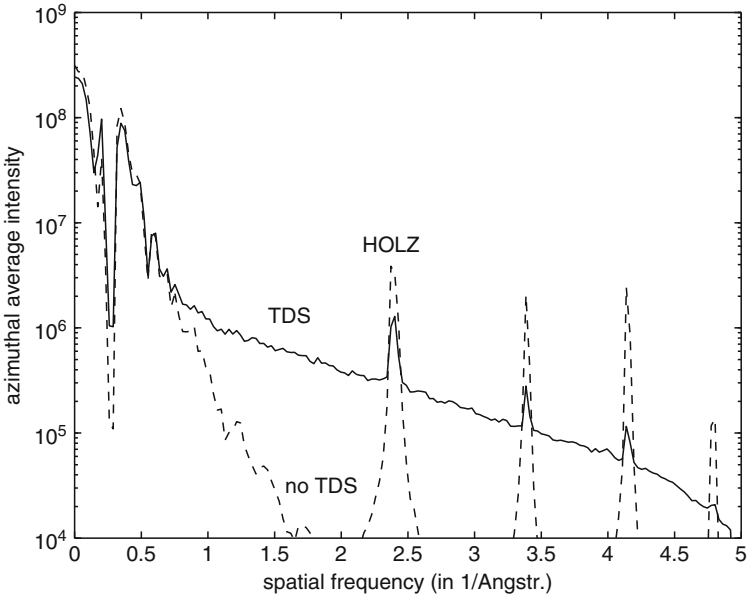

Fig. 7.19 Azimuthal average of the scattered intensity in the simulated CBED diffraction pattern including thermal atomic vibrations in 111 silicon as in Fig. 7.18d. The *solid line* includes thermal vibrations and the *dashed line* does not (Fig. 7.18a)

angles (on the ADF detector) to 290 mrad. The TDS calculation was averaged over 32 phonon configurations. Both calculations include a source size of 0.5 Å (full width half max.), calculated by convolving a 2D image (64 by 256 pixels) with a Gaussian of the appropriate width.

In the top graph (of Fig. 7.20) the atom pairs are nicely resolved and the TDS scattering does not have much effect (overall curve moved up slightly). There is a slight asymmetry due to the stacking order in the two columns, which will likely disappear in practice with surface relaxation of the crytal. The systematic error in this calculation may be about the size of the difference between these two curves so there may not be a real difference in the two curves. The bottom graph includes only high angles on the detector and the TDS scattering has the effect of reducing the overall signal which is a little unexpected. It is likely that there is a strong set of Bragg peaks near the inner angle of the detector (the FOLZ line) whose intensity gets scattered off the detector and disappears. It is not always a good idea to restrict the detector to very high angles. Usually, it's best to get the FOLZ nicely centered on the detector.

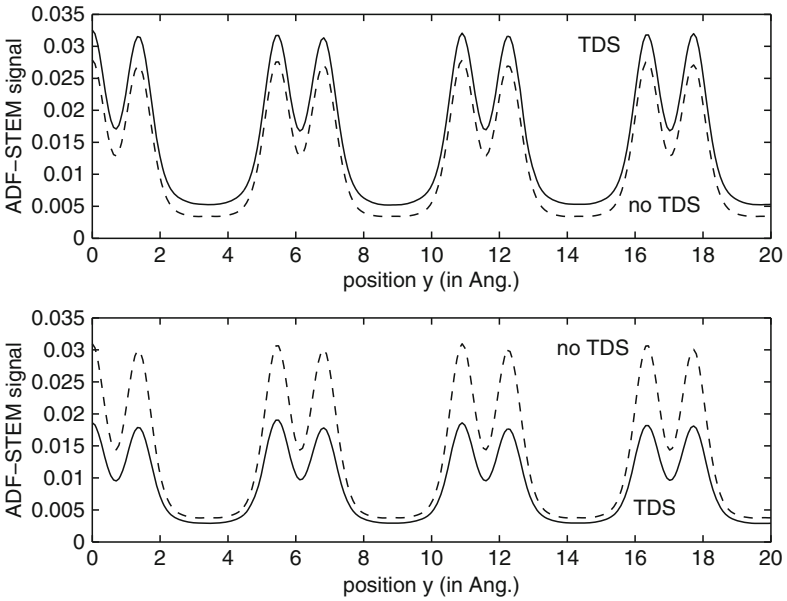

Fig. 7.20 Calculated aberration corrected ADF-STEM images for the 110 projection of silicon with and without TDS scattering, at a beam energy of 100 keV (defocus of 0Å, $C_{S5} = 0$, $C_{S3} = 0$, obj. apert. = 35 mrad). The specimen thickness was 100Å. The area of each image corresponds to 5×4 unit cells of the type shown in Fig. 5.15. The *top graph* has a detector of 80–200 mrad. and the bottom graph has a detector of 120–280 mrad

7.5 Specimen Edges or Interfaces

Calculating images of edges and interfaces presents some special problems. The specimen is no longer really periodic. The so-called wrap-around error causes an extra edge or interface to be introduced (see Fig. 6.13). Figure 7.21 shows the image of a sharp edge of copper. There is a pure crystal of copper in the left half and vacuum in the right half with an atomically sharp edge in the middle. Copper is a simple FCC (face centered cubic) structure with a unit cell size of 3.61Å.The edge could also be an interface between two different materials, with the same problem. There is one intended edge (or interface) in the center and also an unintended interface on the left and right edges due to the wrap around effect. The effects of this edge are just visible along the right edge of each image. Usually only the middle interface is of interest and typically only the middle portion of the image (with left and right edges removed) is shown. However, the whole image is shown here to help understand the situation.

The trick to calculating an edge or interface which is not strictly periodic using an FFT based multislice method in which the specimen is required to be periodic in the two-dimensional image plane is to make the specimen extra long in the nonperiodic direction. The specimen does not have to be periodic along the beam direction (into

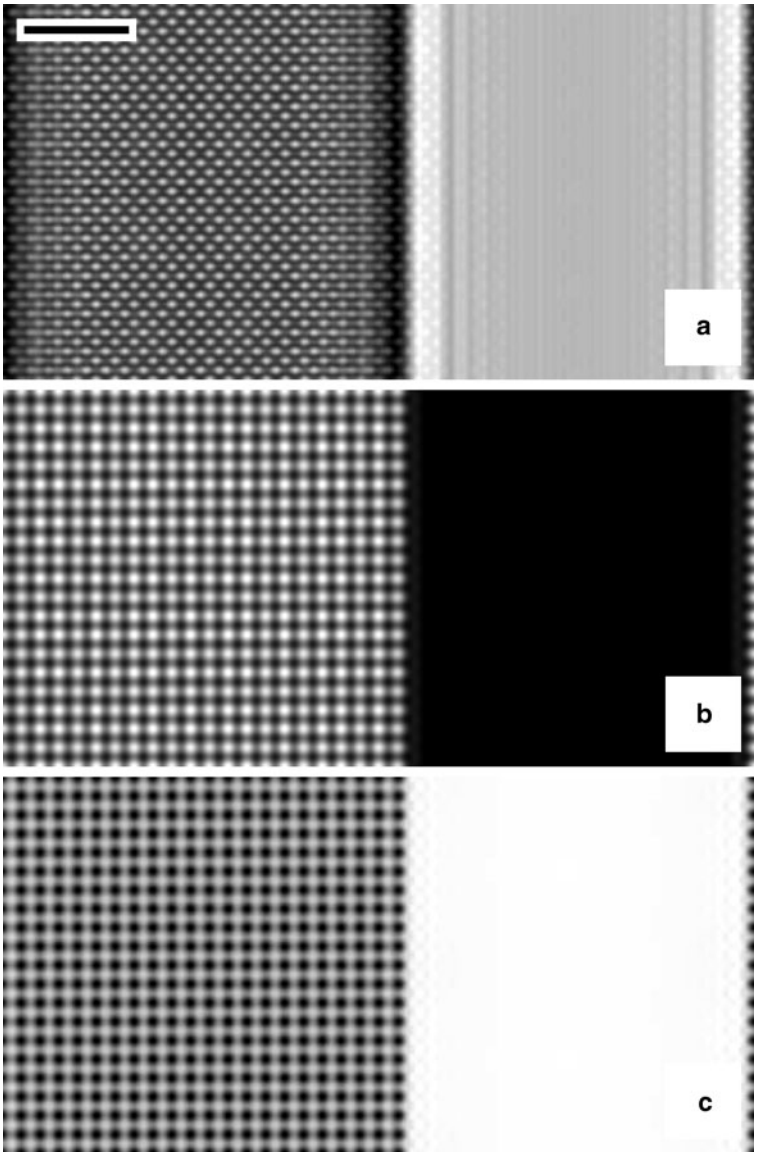

Fig. 7.21 Calcualted images of an edge of copper at 200 kV. (a) BF-CTEM image, (b) ADF-STEM image, (c) confocal STEM with a detector radius of 2Å, and the same paraemters for the collector lens as the objective lens. $C_s = 0.7$ mm. A defocus of 700Å, and an objective aperture of 12 mrad. The scale bar is 10Å

the page in this example). If it is long enough, the two interfaces are far apart and do not interfere with each other. The new unit cell is called a super cell. In this example the super cell is 72.2 by 36.1 Å and was sampled with 512 by 256 pixels

for BF-CTEM and 1024 by 512 pixels for ADF and confocal STEM. The specimen was 50.54 Å thick (thin to reduce thickness effect for simplicity which also reduces the computer time). The STEM probe was sampled with 512 by 512 pixels (which effectively slides around on the larger specimen). Using a smaller sampling for the probe reduces the required computer time (which is significant for this calculation). The final image has 512 by 256 pixels. The atomic columns should appear dark in (a) and (c) and white in (b).

The ADF-STEM image (Fig. 7.21b) is incoherent and the edge appears sharp (white dots at the atom positions). The BF-CTEM image (Fig. 7.21a) is coherent and a well known Fresnel fringe (oscillations) appears at the edge (both edges) which makes it difficult to determine the exact location of the edge. This particular confocal image is well behaved although confocal is frequently not well behaved (in part because there are twice as many parameters to go wrong).

Figure 7.22 show an ADF-STEM experimental image of $SrTiO_3$ grown by pulsed laser deposition in a manner similar to that described by Ohtomo et al. [266] The growth direction is left to right (or right to left) across the page. Single atomically sharp layers of La were deposited and appear as two vertical layers (bright vertical row of dots in the image), in a demonstration of the remarkable control of the growth process using this technique. La has a higher atomic number ($Z = 57$) than Sr ($Z = 38$) so the Z-contrast feature of ADF-STEM produces a larger signal at the La positions ($Z = 22$ and 8 for Ti and O). This image was recorded on a JEOL 2010F at an energy of 200 keV.

To calculate this image, a set of coordinates were generated in three dimensions for 43 by 1 by 1 unit cells of $SrTiO_3$ with the perovskite structure (using a separate short program). One row of Sr atoms was replaced with La atoms at two positions. In reality there will probably be some relaxation of the atomic coordinates about this layer but this has been ignored. When the program was run it expanded in thickness (z) and height (y) to 22 by 26 unit cells to get a total thickness of about 100 Å. For the ADF-STEM calculation (Fig. 7.23b), the specimen was sampled with 4096 by 2048 pixels and the probe was sampled with 512 by 512 pixels. The ADF detector extended from 40–200 mrad. and the image was calculated for 512 by 256 pixels. The final image was convolved with a Gaussian low pass filter to approximate a 1.5Å source size (in the specimen plane). The BF-CTEM image (Fig. 7.23a) was calculated with 2048 by 1024 pixels. Figure 7.23 shows the calculated images to match Fig. 7.22. There is reasonable qualitative agreement. The ADF-STEM image yields a slightly more directly interpretable image at the La layers.

7.6 Biological Specimens

The multislice method is capable of handling specimens that are nearly amorphous. Each slice of the specimen is calculated independently of the other slices so the specimen can be completely amorphous in the beam direction (z as used in this

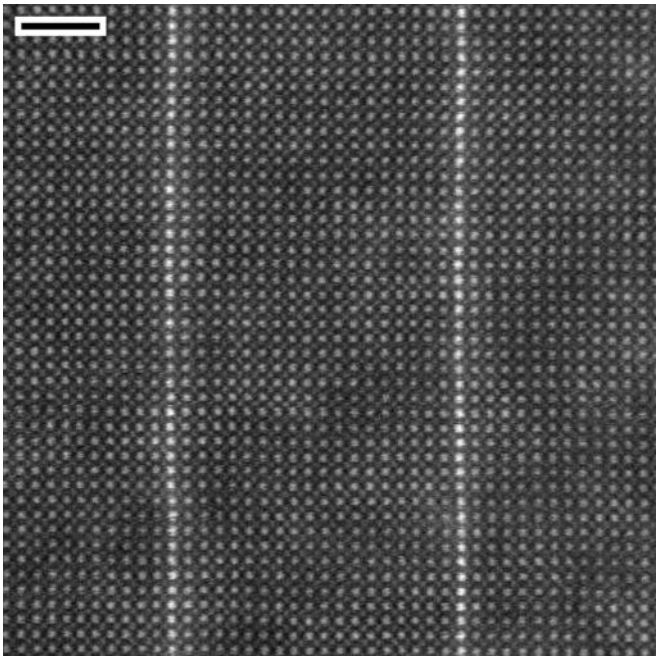

Fig. 7.22 Experimental 200 keV ADF-STEM image of single layers of La in strontium titanate ($SrTiO_3$) $C_s = 1.0$ mm and an objective aperture of 10 mrad. The scale bar is 20Å. (Courtesy of D. A. Muller, previously unpublished)

book). Using a discrete Fourier transform (the FFT) in two-dimensions perpendicular to the beam direction forces the unit cell to be repeated infinitely in those two direction (x, y as used in this book). If the specimen is somehow bounded (such as a nano particle or macromolecule) and embedded in a larger supercell such that the repeated copies of the specimen are far apart so they do not interfere with each other then amorphous objects may be calculated using the multislice method (see Fig. 6.12).

Biological macromolecules or microorganisms are good examples of amorphous particles (the method discussed next will also apply to inorganic nano particles as well). The Protein Data Base (PDB) is an on-line depository of structure data for proteins and related molecules, many of which come from X-ray diffraction studies of crystallized specimens. Each structure data file in the PDB contains a list of atomic coordinates (in three dimensions) that can be converted to a format used here for a multislice calculation (as done by Wall [363]). The image of α-hemolysin (PDB identification 7AHL.pdb, Song et al. [328]) is calculated in Fig. 7.24. This molecule has 22,778 atoms and is projected along the z axis as defined by the PDB file (which does not seem to be along the primary symmetry axis, but tilted slightly). Several major effects will be ignored for simplicity. Radiation damage is frequently the primary limiting factor in images of biological specimens. The total beam dose

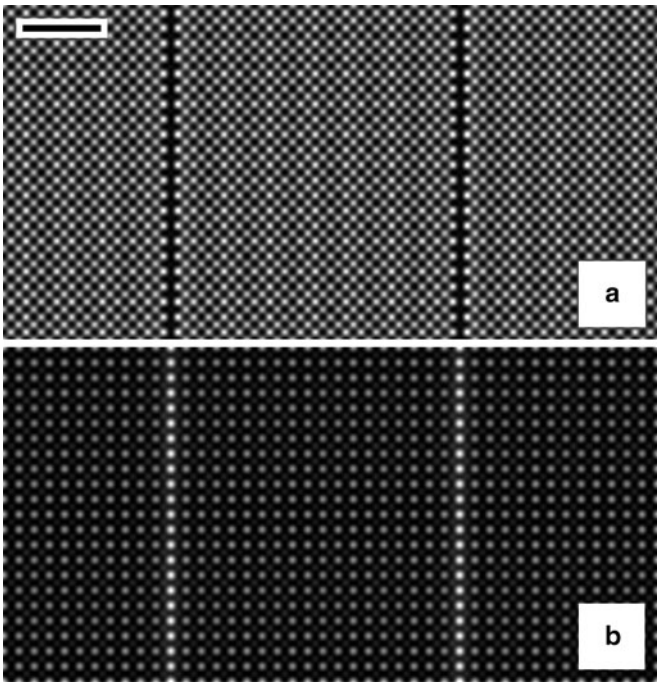

Fig. 7.23 Calculated 200 keV ADF-STEM image of single layers of La in strontium titanate ($SrTiO_3$) $C_s = 1.0$ mm and an objective aperture of 10 mrad. (a) BF-CTEM and (b) ADF-STEM with a 1.5Å source size. The scale bar is 20Å

must be limited to some small value. Part of the specimen may be moved around by the interaction with the beam if it has too large of a current. The low dose generates at lot of noise in the image. Both of these effect are ignored here for simplicity, so this result is a little bit of a fantasy.

Figure 7.24a is a BF-CTEM image (512 by 512 pixels) of the molecule with no support (magically suspended in space). Figure 7.24b is a BF-CTEM image of the molecule with a 20Å amorphous carbon support, simulated by generating uniformly distributed random numbers inside a rectangular slab on the exit surfaces used as atomic coordinates for the carbon atoms maintaining a minimum separation of 1Å and the known density of carbon. There were a little over 53,000 atoms in the carbon support. There is essentially nothing visible in the BF image, which is why biological specimens are usually stained with some heavy material (no stain here). In principle multislice can handle a surrounding stain if given a list of coordinates for the atoms in the stain (not easy to get or calculate). Figure 7.24c is an ADF-STEM (40–100 mrad detector) image and Fig. 7.24d is a confocal image. The specimen transmission functions (one per 2Å slice) were sampled with 2048 by 2048 pixels and the probe was 512 by 512 pixels. There are 256 by 256 pixels in the

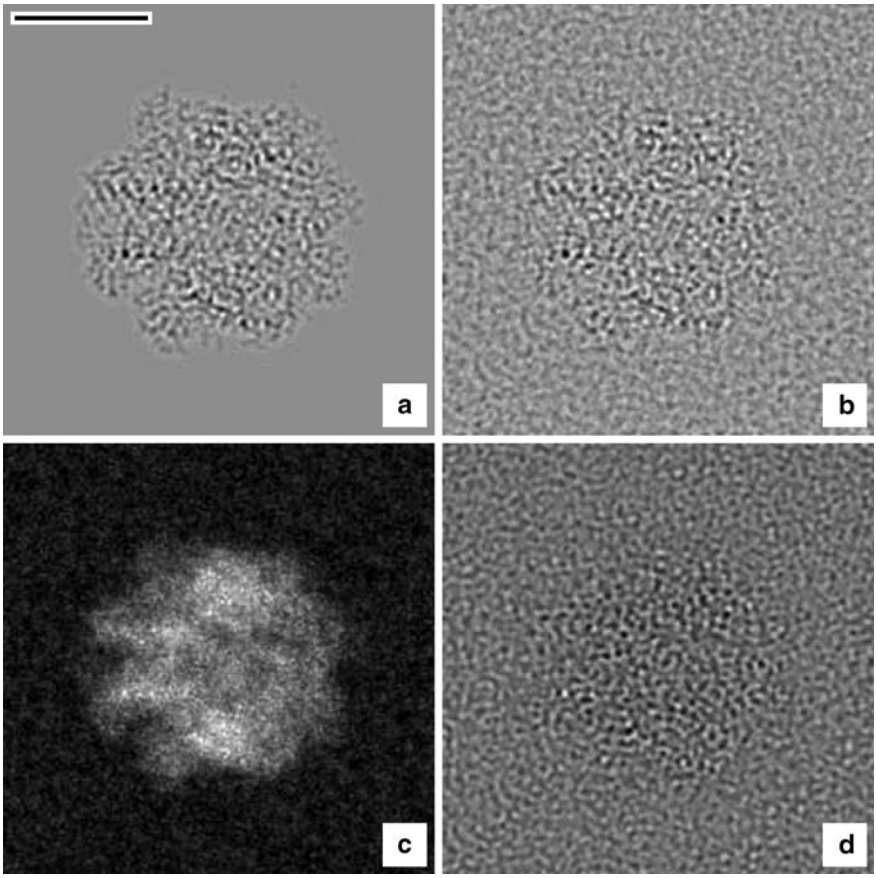

Fig. 7.24 Calculated images of α-Hemolysin(Song et al. [328] (a,b) BF-CTEM, (c) ADF-STEM and (d) SCEM (confocal). (a) Has no carbon support (not physically possible) and (b–d) have a 20Å amorphous carbon support. Electron beam energy 200 keV, $C_S = 1.3$ mm, $\Delta f = 700$Å, obj. apert. 10 mrad, confocal collector lens was similar to obj. lens. and used a 2Å diameter detector. Radiation damage and low beam dose noise are ignored for simplicity. The scale bar is 50Å

final image. It is interesting that the structure should be vivible even without staining in ADF. There might be some reason to try this with a low dose technique and a cold stage to reduce radiation damage. For this particular specimen and imaging parameters the simple incoherent image model (3.66) yields an image that is subjectively the same as the image in Fig. 7.24c, which can be calculated in seconds rather than hours. Engel and Colliex [94] and Engel [93] (amongst many) have reviewed STEM imaging of biological specimens. BF-CTEM imaging of biological specimens has been reviewed by a great many authors.

7.7 Quantitative Image Matching

Most comparisons between theoretically simulated electron micrographs and experimentally recorded electron micrographs are somewhat subjective. The two images are just displayed side by side and pronounced as being in good agreement after subjective visual inspection (Sect. 7.3 is also guilty of this practice). In principle it is possible (indeed recommended) to be more quantitative in comparing simulated and recorded images (Barry [19, 20]). An easily definable figure of merit is the Chi-Squared measure of the difference between two images:

$$\chi^2 = \frac{1}{N_x N_y} \sum_{i,j} [f_{\text{exp}}(x_i, y_j) - f_{\text{sim}}(x_i, y_j)]^2 / \sigma_{ij}^2, \tag{7.1}$$

where $N_x N_y$ is the number of pixels in the image, σ_{ij} the error associated with pixel (i, j), $f_{\text{exp}}(x_i, y_j)$ the experimental image, and and $f_{\text{sim}}(x_i, y_j)$ is the simulated image. (This symbol χ should not be confused with the same symbol used for the aberration function.) This definition of χ^2 is technically called the reduced χ^2 because it is normalized to the total number of data points. A value of $\chi^2 \sim 1$ indicates a good fit. The r-factor figure of merit (R_1, or R_2) commonly used in X-ray diffraction could also be used.

$$\begin{aligned} R_1 &= \int |f_{\text{exp}}(x,y) - f_{\text{sim}}(x,y)| \mathrm{d}x\mathrm{d}y \Big/ \int |f_{\text{exp}}(x,y)| \mathrm{d}x\mathrm{d}y \\ R_2 &= \int |f_{\text{exp}}(x,y) - f_{\text{sim}}(x,y)|^2 \mathrm{d}x\mathrm{d}y \Big/ \int |f_{\text{exp}}(x,y)|^2 \mathrm{d}x\mathrm{d}y. \end{aligned} \tag{7.2}$$

It would be very nice to be able to quote a value of χ^2 or the r-factor for the agreement between a simulated image and an experimentally recorded image. However, there are considerable obstacles to overcome to perform a quantitative image match. In practice the two images to be compared can be in different orientations (translation and rotation) and they will never be at exactly the same magnification. Just to begin a quantitative comparison requires fitting these four degrees of freedom. These properties of the image must be found in spite of the fact that the image may be noisy.

Next the overall scale and background level of the experimental image must be found. Most image detectors (film is particularly difficult to quantify) are designed to provide a linear image which is all that is required for human vision. This means that there are two additional degrees of freedom. The recorded image intensity may have an arbitrary additive and multiplicative constant:

$$f_{\text{exp}}(x,y) = a_{\text{det}} f_{\text{ideal}}(x,y) + b_{\text{det}}, \tag{7.3}$$

where a_{det} and b_{det} are constants unique to each detector. These scaling constants can be found by recording the image intensity through a hole in the specimen and

the intensity with the beam turned off (ideally at the same time that the image is recorded), but this additional measurement is rarely done. Film and plates notoriously vary with development time and temperature etc. and are difficult to quantify but more modern CCD imaging systems may make this much easier. With a lot of care an experimental image can be recorded with sufficient detail to quantitatively compare to a simulated image but this extra burden is rarely accepted in practice, so most comparisons are subjective in nature.

Thust and Urban [344] and Möbus and Rühle [250] have also proposed using the cross correlation coefficient such as:

$$C_{\mathrm{cor}}(f_{\mathrm{exp}}, f_{\mathrm{sim}}) = \frac{\sum_{xy}(f_{\mathrm{exp}}(x,y) - f_{e0})(f_{\mathrm{sim}}(x,y) - f_{s0})}{\sqrt{\sum_{x,y}(f_{\mathrm{exp}}(x,y) - f_{e0})^2 \sum_{xy}(f_{\mathrm{sim}}(x,y) - f_{s0})^2}}, \tag{7.4}$$

where f_{e0} and f_{s0} are the average values of $f_{\mathrm{exp}}(x,y)$ and $f_{\mathrm{sim}}(x,y)$, respectively. The cross correlation coefficient has the advantage of eliminating the dependence on the scaling parameters of the detector.

Minimizing χ^2 (or maximizing the cross correlation coefficient) with respect to some parameter of the simulation is a method for extracting that parameter from the recorded image. The specific program implementation of a minimization procedure can become rather involved and may involve a multislice simulation for each iteration. Kirkland [210] has used this approach to determine the defocus of the electron micrographs. Wilson et al. [382] have used a semiquantitative matching technique to determine the optical parameters of the microscope such as spherical aberration C_s and defocus Δf.

Ourazd et al. [278] have used a quantitative pattern matching technique to map the stoichiometry of their specimen. A precalculated set of possible specimen types was quantitatively compared to each unit cell of the specimen to determine its chemical composition. The best match determined the chemical composition of each unit cell. This requires that there be a small number of different unit cells.

King [198] and Möbus and Rühle [250] have perform nonlinear least squares fitting to extract specimen parameter such as tilt and defocus as well as the atomic coordinates. Zhang et al. [392] have uses a quantitative fitting procedure to refine the atomic coordinates at an interface. Möbus [247] and Möbus and Dehm [248] have recently proposed maximizing the cross correlation coefficient instead of minimizing χ^2 to refine the specimen parameters and coordinates. Möbus et al. [251] have presented a general structure retrieval program using image matching.

For the last decade or so many authors have found a significant discrepancy of about a factor pf 2X to 3X (principally in the lattice fringe amplitude) between calculated and experimentally measured images that has become known as the "Stobbs factor" (Hÿtch and Stobbs [167], Boothroyd [33]). As discussed earlier this is a difficult measurement, usually requiring a measurement of the incident beam intensity on an absolute scale, an accurate specimen model and a well characterized electron optical column (aberrations and partial coherence) and detector response function. A possible amorphous contamination layer (Mkoyhan et al. [246]) on the specimen (usually organic material from the air or diffusion pumps), crystal tilt (Maccagnano

et al. [232]) or inelastic scattering may also confuse the issue. Thust [343] has recently obtained good quantitative agreement of BF-CTEM images using an accurate model of the CCD transfer function. Klenov et al. [213], and LeBeau et al. [223] have also obtained good agreement between measured and calculated ADF-STEM images using Bloch waves and multislice with the frozen phonon approximation. There is good reason to believe that the current theory is quantitatively correct with careful attention to experimental details.

7.8 Troubleshooting (What Can Go Wrong)

There are a large number of things that can go wrong in an image simulation. The proposed specimen structure must be specified in some detail, usually in the form of a list of atomic coordinates and atomic numbers in a unit cell. Even less well known is the thickness of the specimen. Usually, a large sequence of possible specimen thicknesses is calculated and compared to experiment.

The instrumental (optical) parameters such as the aberration constants (C_s, etc.) and aperture size of the objective lens and lens defocus must be known. Usually defocus is not know very well (particularly in bright field phase contrast). Frequently, a *defocus series* is calculated for comparison to experiment. There are also a variety of parameters such as defocus spread, illumination angle, etc. that are hard to estimate but can influence the image.

There are also many parameters that are solely related to the calculation and have very little to do with the microscope or specimen but can dramatically affect the calculation. These parameters include the sampling size (pixel size) in the image and slices and the slice thickness itself.

Multislice almost always uses an FFT to reduce the total CPU time. The FFT is a discrete Fourier transform which repeats the image infinitely in all directions. Although the image is only displayed as a single image you should remember that it is really an infinite array of identical side-by-side images. This produces a strange effect called the *wrap-around error*. The left side of the image in essence touches the right side of the image (and vice versa) and the top of the image touches the bottom of the image (see Fig. 6.12). To use the FFT each image and slice must obey periodic boundary conditions or be an integer number unit cells of the specimen (called a super cell). Interfaces and defects must be imbedded inside a large super cell.

In summary, some of the things that need to be specified correctly are:

Specimen parameters: atomic coordinates and numbers of the specimen and thickness of specimen

Instrumental parameters: defocus, C_s, objective aperture, etc.

Sampling size: number of pixels in the image and slice and the slice thickness. Ensure that the total integrated intensity is at least 0.9 or higher (1.0 to start). Calculations with slightly higher or lower sampling should yield the same result if the sampling is adequate.

Slice thickness: usually the slices should correspond to the existing atomic layers in the specimen. If the slices are too thick then the total integrated intensity will decline too much (as in the sampling size issue) and may produce false high order Laue zones corresponding to the slice thickness.

Wrap-around error: each slice must obey periodic boundary conditions.